



# Atomic-scale Insights into the Effects of Diffusion on the Binding of Adsorbed Sodium on the Surfaces of the Moon and Mercury

Anastasis Georgiou<sup>1</sup> , Amanda Ricketts<sup>1</sup> , Jason McLain<sup>2</sup>, Sébastien Verkerke<sup>3</sup> , François Leblanc<sup>4</sup> , Menelaos Sarantos<sup>5</sup> , and Liam S. Morrissey<sup>1</sup>

<sup>1</sup> Faculty of Engineering and Applied Science, Memorial University of Newfoundland, St. John's, NL A1C 5S7, Canada

<sup>2</sup> NASA Goddard Space Flight Center, Greenbelt, MD 20771, USA

<sup>3</sup> LATMOS/CNRS, Université Versailles Saint Quentin, Guyancourt, France

<sup>4</sup> LATMOS/CNRS, Sorbonne Université, Paris, 75252, France

<sup>5</sup> Heliophysics Science Division, NASA Goddard Space Flight Center, Greenbelt, MD 20771, USA

Received 2025 April 30; revised 2025 July 11; accepted 2025 July 12; published 2025 August 26

## Abstract

The collisionless atmospheres of the Moon and Mercury allow for different space weathering processes to occur on their surfaces. During these processes, atoms can be ejected ballistically into the exosphere, a portion of which will eventually return to the surface. These returning atoms can then adsorb on the surface with a binding energy (BE) different than that of the mineral. However, it is unknown how adsorbates sample the different possible binding sites on the surface, or how diffusion can dynamically affect the BEs and eventual desorption process. Here, we conduct molecular dynamics simulations of the adsorption, diffusion, and desorption of sodium (Na) atoms on different silicates relevant to the Moon and Mercury. We consider the effect of crystallinity and temperature on the BE and diffusion behavior of adsorbed Na over time. Results show that Na adsorption strongly depends on the surface mineral composition and the presence of bridging and nonbridging oxygen. Na on silica surfaces had the highest adsorption energy compared to albite and anorthite due to the higher proportion of exposed nonbridging oxygens on the surface. We also observe that the BE increases as the Na atoms are allowed to diffuse and desorb. This suggests that while adsorbates may initially randomly sample different binding sites, with time they will diffuse toward high-BE sites. Finally, our simulations show that with an increase in temperature, there is an increased probability of desorption.

*Unified Astronomy Thesaurus concepts:* Mercury (planet) (1024); The Moon (1692); Planetary surfaces (2113); Surface processes (2116); Exosphere (499)

## 1. Introduction

The collisionless atmospheres of the Moon and Mercury allow for several space weathering processes, such as micro-meteoroid impact vaporization and solar wind ion sputtering, to take place concurrently on their surfaces. Many of these processes can lead to the emission of surface atoms into the exosphere. Observations of atoms in the exospheres of airless bodies are widely considered to originate from these space weathering events (A. L. Broadfoot et al. 1976; T. A. Cassidy et al. 2016; R. J. Vervack et al. 2016; E. Quémérais et al. 2023). Other processes, such as photon-stimulated desorption (PSD), electron-stimulated desorption (ESD), and thermal desorption, are also likely important mechanisms that could eject atoms to the exosphere (D. L. Domingue et al. 2014).

Initial observations of neutral species in the exosphere of Mercury were detected by the Mariner 10 Ultraviolet Spectrometer, which discovered traces of hydrogen and helium originating from the solar wind (A. L. Broadfoot et al. 1976). A decade later, ground-based observations by A. Potter & T. Morgan (1985, 1986) discovered exospheric sodium (Na) and potassium, followed by the discovery of calcium (Ca) years later (T. A. Bida et al. 2000). The MErcury Surface, Space ENvironment, GEochemistry, and Ranging (MESSENGER) spacecraft performed three flybys of Mercury, detecting

exospheric magnesium (Mg) and ionized Ca through its Mercury Atmospheric and Surface Composition Spectrometer (MASCS) instrument (W. E. McClintock et al. 2009; R. J. Vervack et al. 2010). Aluminum was initially observed by A. Doressoundiram et al. (2009) and later measured by T. A. Bida & R. M. Killen (2011), who also reported observations of iron (Fe) through ground-based instruments. MESSENGER/MASCS also confirmed the presence of aluminum in the exosphere, but Fe was not observed (R. J. Vervack et al. 2016). The same observations by R. J. Vervack et al. (2016) also reported the first manganese detection while confirming previous ionized Ca measurements. The recent BepiColombo mission also observed Ca and Mg (R. Robidel et al. 2023).

Of the several atomic species discovered, Na remains the most studied and abundant in Mercury's exosphere. Several different space weathering processes are thought to be potentially important for its ejection into the exosphere, however the exact contribution of each remains unknown (T. E. Madey et al. 1998; B. V. Yakshinskiy et al. 2000; F. Leblanc & R. E. Johnson 2003; B. V. Yakshinskiy & T. E. Madey 2003; R. M. Killen et al. 2004; M. Sarantos & S. Tsavachidis 2020; P. Wurz et al. 2010). In addition, those atoms ejected with an energy below the escape energy can return to the surface and adsorb at binding energies (BEs) lower than when bound within the mineral (L. S. Morrissey et al. 2025). Due to their lower BEs, these can be more efficiently re-ejected through less energetic processes such as PSD, ESD, and thermal desorption.



Original content from this work may be used under the terms of the [Creative Commons Attribution 4.0 licence](#). Any further distribution of this work must maintain attribution to the author(s) and the title of the work, journal citation and DOI.

The relative efficiency of each of these desorption processes has been widely discussed among the scientific community. Early suggestions show that photons, through PSD and thermal desorption, are largely responsible for transporting adsorbed Na to the exosphere (M. A. McGrath et al. 1986). This was further strengthened through observations of a morning and afternoon Na emission that was interpreted as thermal desorption (A. L. Sprague 1992). Experiments by B. V. Yakshinskiy et al. (2000) showed that thermal desorption is efficient at temperatures greater than 400 K for adsorbed Na on thin silica films. Considering the results by B. V. Yakshinskiy et al. (2000), F. Leblanc & R. E. Johnson (2003) suggested that thermal desorption could lead to rapid depletion of the adsorbed Na from the surface, limiting other ejection processes such as PSD and solar wind sputtering. In contrast, T. A. Cassidy et al. (2016) suggested that depletion of the adsorbed Na would only be partial.

Despite the progress made in modeling Mercury's exosphere using experimental results, there are still many assumptions underlying these results that often do not fully capture the complexities of the surface of Mercury. For example, the collisional sputtering processes contributing to exosphere formation are still not completely understood, particularly regarding the ejected atoms' energy distributions and the influence of surface binding energies (SBEs) (R. M. Killen et al. 2022; L. S. Morrissey et al. 2022; N. Jäggi et al. 2024; L. S. Morrissey et al. 2024). More recently, atomistic modeling, such as molecular dynamics (MD) simulations, has been used to study the SBEs of different elements as a function of mineral type and orientation, providing a more accurate prediction of the sputtering yields (L. S. Morrissey et al. 2022; L. S. Morrissey et al. 2024). L. S. Morrissey et al. (2025) used MD modeling to study the SBEs of Na adsorbates on  $\text{SiO}_2$  as a function of coverage. Results showed that the SBE was highly dependent on the coverage, and that a wide range of SBEs were possible. They concluded that Na appeared to randomly sample the different binding sites available on the surface. Previous studies have also used MD to study the adsorption of Na and metals on silicate surfaces; however, they have focused on the general adsorption mechanism and do not provide a value for the adsorption energies (S. H. Garofalini & D. M. Zirl 1988; D. C. Athanasopoulos & S. H. Garofalini 1992). While these studies have demonstrated the potential of MD for studying adsorbates, they assume that the binding sites being sampled initially represent a stable configuration which can be used in subsequent larger-dimensional-scale models. It is unknown whether diffusion of adsorbates along the surface can dynamically affect the BEs. Are adsorbates randomly sampling the different binding sites, or, with time and temperature, can they diffuse and preferentially sample specific sites? The answers to these questions may have important implications for adsorbate reservoirs on the surfaces of airless bodies (S. Verkerke et al. 2024). Here, we use MD modeling to study the dynamic behavior of Na adsorbates on the surfaces of key silicates and feldspars relevant to the Moon and Mercury. Our simulations consider the atomic mechanism of adsorption, allowing the adsorbates to diffuse and eventually desorb with time. We investigate how the distribution of BEs changes with temperature, time, crystallinity, and surface composition.

## 2. Methodology

### 2.1. Molecular Dynamics Simulations Details

MD is a deterministic numerical method used to simulate the behavior of atoms in a system with time. Newton's second law is used to derive the dynamics in MD, which are computed at a given time step and combined with the initial atomic positions and velocities to generate new positions and velocities. To calculate the behavior of a system from Newton's laws, MD also requires an inter-atomic potential to describe the forces of the interacting atoms. The accuracy of results strongly depends on the ability and accuracy of the inter-atomic potential used to describe the inter-atomic interactions.

Here, MD simulations were carried out using the Large-scale Atomic/Molecular Massively Parallel Simulation (or LAMMPS) package (S. Plimpton 1995). A reactive force field (ReaxFF) empirical potential (A. C. T. Van Duin et al. 2001) was used to describe the interactions between atoms along with the charge equilibration (QeQ) method (H. M. Aktulga et al. 2012). The ReaxFF potential is a bond-order-based potential, allowing for bonds to dynamically break and reform during the simulation. It can describe chemical bonds of systems without expensive quantum mechanics calculations (T. P. Senftle et al. 2016). More details regarding the ReaxFF potential are given in A. C. T. Van Duin et al. (2001). The selected ReaxFF potential was initially developed by M. C. Pitman & A. C. T. Van Duin (2012) for clay zeolites. This potential was extensively validated by Y. Yu et al. (2017) for its ability to accurately predict key properties for different sodium silicates beyond what it was initially parameterized for. Y. Yu et al. (2017) modeled sodium silicate glass and compared the predicted structure to those obtained by classical potentials, ab initio methods, and experiment. They concluded that ReaxFF, owing to its bond-order form, can accurately predict the different structures and demonstrates good transferability to other compositions. Building on these findings, the chosen ReaxFF potential was used by G. A. Lyngdoh et al. (2019) for geopolymers, R. A. Mayanovic et al. (2023) for albite, and L. S. Morrissey et al. (2024) to calculate the SBE of elements in albite and anorthite.

### 2.2. Preparing the Silicate Structures

We performed MD simulations on the two end-members of the plagioclase feldspar group, albite ( $\text{NaAlSi}_3\text{O}_8$ ) and anorthite ( $\text{CaAl}_2\text{Si}_2\text{O}_8$ ), which are thought to be abundant on the surface of the Moon and Mercury (D. S. McKay et al. 1991; A. L. Sprague 1992; D. L. Domingue et al. 2014). We also considered silica ( $\text{SiO}_2$ ), which is found on Mercury's surface at 49–55 wt% (A. L. Sprague et al. 1994). First, to create crystalline samples we replicated the crystallographic information files (or CIFs) for each mineral type, obtained from the Materials Project (A. Jain et al. 2013), to final dimensions of  $\sim 55 \times 53 \times 38 \text{ \AA}^3$ . We used  $\alpha$ -quartz as the crystalline form of  $\text{SiO}_2$ . These crystalline structures were then relaxed and equilibrated in an isobaric-isothermal NPT (number of particles, pressure, temperature) and then an NVT (particles, volume, temperature) ensemble to the desired temperatures (100, 300, and 700 K) and pressures (0 atm). The simulation domain was then extended 60 Å in the (001)  $z$ -direction. Boundary conditions were set to periodic in the  $x$ - and  $y$ -directions with a fixed boundary condition in the  $z$ -direction, simulating an infinite slab with constant

**Table 1**  
System Characteristics and Validation

Number of Atoms	Temperature (K)	Density ( $\text{g cm}^{-3}$ )			
		MD Simulation		Experimental (300 K)	
		Crystalline	Amorphous	Crystalline	Amorphous
Silica	7560	100	2.640	2.146	...
		300	2.609	2.125	2.65 <sup>a</sup>
		700	2.537	2.078	... 2.21 <sup>a</sup>
Albite	7767	100	2.604	2.224	...
		300	2.588	2.209	2.62–2.65 <sup>a</sup> , 2.615 <sup>b</sup> ,
		700	2.554	2.171	... 2.382 <sup>b</sup> , 2.285 ± 3 <sup>c</sup>
Anorthite	8736	100	2.754	2.533	...
		300	2.777	2.532	2.74–2.76 <sup>a</sup> , 2.763 <sup>b</sup> ,
		700	2.786	2.524	... 2.691 <sup>c</sup>

#### Notes.

- <sup>a</sup> W. M. Haynes (2014).
- <sup>b</sup> M. Taylor & G. E. Brown (1979).
- <sup>c</sup> M. Dal Bó et al. (2013).

thickness and a free surface. The (001) surface was chosen as it is the perfect cleavage plane due to its uniformity and minimal broken bonds (J. W. Anthony et al. 2001). The bottom 3 Å of each slab was fixed in space so they did not shift during the simulations.

Next, amorphous samples were prepared following the methods described by L. S. Morrissey et al. (2022a) and A. Pallini et al. (2023), who studied amorphous silicate structures. Starting from a crystalline structure, each sample was first equilibrated to 100 K using a Nose–Hoover thermostat with an NVT ensemble. The systems were then heated to 4000 K and kept at that temperature for 85 ps before being cooled back down to 100 K in an NVT ensemble. Next, the systems were again heated to 4000 K in an NPT ensemble and kept at that temperature for 85 ps before being cooled back down in an NPT ensemble. After the amorphization stage, the structures were equilibrated to the desired temperatures with boundary conditions similar to the crystalline systems to create an infinite slab. To validate these methods, we compared the final densities of each case to the available experimental data, as seen in Table 1.

### 2.3. Calculating Adsorption Energy

After the preparation of each slab, ~240 Na atoms were then randomly placed at 5 Å above the surface, similar to previous Na adsorption studies (D. C. Athanasopoulos & S. H. Garofalini 1992; M. Rarivomanantsoa et al. 2004). The Na atoms were then allowed to adsorb on the surface in an NVT ensemble for 100 ps at 100, 300, and 700 K. Temperatures were chosen to match those typically observed on Mercury, which can be as low as ~100 K on the nightside (S. C. Chase et al. 1976) to ~700 K on the dayside (D. Morrison 1970). 300 K was selected as an intermediate temperature, which is typically observed at Mercury’s terminators and on the dayside at high latitudes close to the poles (A. R. Vasavada et al. 1999; F. Leblanc et al. 2023; S. Verkercke et al. 2024). The simulation time step was set to 0.0005 ps, similar to previous adsorption studies (P. P. Liu et al. 2019; M. Hajianzadeh et al. 2023). After 100 ps, the Na

adsorption energy was calculated using Equation (1):

$$E_{\text{ads}} = \frac{E_{\text{Na+slab}} - (E_{\text{slab}} + E_{\text{Na}})}{N_{\text{Na}}}, \quad (1)$$

where  $E_{\text{ads}}$  is the adsorption energy,  $E_{\text{Na+slab}}$  is the total energy of the adsorbed Na atoms and the slab,  $E_{\text{slab}}$  is the total energy of the slab without the adsorbed sodium,  $E_{\text{Na}}$  is the total energy of the adsorbed Na atoms without the slab, and  $N_{\text{Na}}$  is the number of adsorbed Na atoms.

### 2.4. Calculating Binding Energy and Diffusion

After the initial adsorption energy at time zero, each setup was then kept at the desired temperature for an additional 4000 ps. This simulated duration was longer than previous silicate diffusion studies (A. H. Quadery et al. 2015; S. A. Sheikholeslam et al. 2016; L. S. Morrissey et al. 2022a; N. T. Thao et al. 2023; N. T. Nhan et al. 2024), which have noted the importance of sample size and statistics to accurately study the atomically random nature of diffusion. The Na atoms’ BE was calculated every picosecond using Equation (1). The BE can be described as the negative of the adsorption energy ( $E_{\text{BE}} = -E_{\text{ads}}$ ). We note that this value is similar but different to the SBE, which is specifically the energy in the normal direction needed to “pull” an atom from the surface such that it no longer interacts with the substrate. We also tracked the mean squared displacement (MSD) of the Na atoms following similar MD studies (L. S. Morrissey et al. 2022a) using Equation (2):

$$\text{MSD} = \frac{1}{N_{\text{Na}}} \sum_{i=1}^N |\mathbf{x}^i(t + t_0) - \mathbf{x}^i(t_0)|^2, \quad (2)$$

where  $N_{\text{Na}}$  is the number of Na atoms,  $\mathbf{x}^i(t)$  represents the position vector of the  $i$ -th particle at an initial time  $t_0$ , and  $\mathbf{x}^i(t + t_0)$  is the position vector of the  $i$ -th particle at a later time  $t + t_0$ . The MSD was calculated in 50 ps intervals for each temperature from 0 to 4000 ps. We note that atoms which cross the periodic boundary are not included in the calculation of the MSD. Atoms which have desorbed and no longer

**Table 2**  
Adsorption Energy Results of Adsorbed Na for Different Temperature Ranges and Silicates

Temperature(K)	Crystalline		Amorphous	
	% of Atoms Adsorbed	Adsorption Energy (eV)	% of Atoms Adsorbed	Adsorption Energy (eV)
Silica	100	54.9	$-4.79 \pm 0.69$	53.9
	300	55.3	$-5.13 \pm 0.73$	51.4
	700	57.4	$-5.08 \pm 0.59$	53.9
Albite	100	60.3	$-3.81 \pm 0.74$	52.0
	300	60.7	$-3.79 \pm 0.70$	51.4
	700	58.3	$-3.89 \pm 0.66$	56.2
Anorthite	100	64.8	$-3.08 \pm 0.78$	54.4
	300	66.4	$-3.14 \pm 0.66$	56.4
	700	77.6	$-3.10 \pm 0.60$	55.6

**Note.** Errors are  $\pm 1$  standard deviation.

interact with the surface are also not included in the MSD calculation.

### 3. Results and Discussion

#### 3.1. Initial Adsorption Energy

MD simulations were used to calculate the adsorption energy of Na on different silicates as a function of temperature. Table 2 shows the initial mean adsorption energy ( $\pm 1$  standard deviation) of Na after the adsorbed atoms settled onto the surface ( $\sim 100$  ps). In all cases the adsorption energies are negative, indicating thermodynamically favorable binding between the Na atoms and the silicate substrates. For crystalline substrates, we observe the formation of a monolayer of Na on the surface, terminating most exposed oxygen (O) atoms. This is more difficult to track in the amorphous case, where randomness and surface roughness dominate. The formation of an Na monolayer bonding with O on the crystalline surfaces suggests that chemisorption is present (A. Thakur et al. 2022; H. Chakhtouna et al. 2023). Chemisorption was also observed by Q. Liu et al. (2021), who used MD simulations to study the adsorption of Na on orthoclase silicate ( $KAlSi_3O_8$ ) surfaces. Similarly, experiments by B. V. Yakshinsky et al. (2000) of Na on amorphous  $SiO_2$  found BEs of  $> 1$  eV, higher than the BE for physisorption ( $< 1$  eV). Recent experimental results by J. L. McLain et al. (2024) of Na/K on high-carbon-content Apollo lunar samples also suggest that Na preferentially fills the chemisorption sites of the samples. Therefore, the high adsorption energy values simulated here further support the idea that adsorption of Na occurs via chemisorption.

We also observe a clear difference in the adsorption energies when comparing the different silicates simulated. For silica, the average adsorption energy across all temperatures was  $-4.95$  eV, 22% and 46% higher than albite and anorthite, respectively. These differences in energy between mineral types can likely be explained by the characteristics of exposed O atoms on the surface. S. H. Garofalini & D. M. Zirl (1988) and D. M. Zirl & S. H. Garofalini (1990) performed MD simulations on silica and sodium aluminosilicates, and found that Na and other alkalies had higher adsorption energies when bonded to nonbridging oxygens (NBOs) rather than bridging oxygens (BOs). When inspecting our surfaces, we can see that silica has 80% more NBOs on the surface compared to crystalline albite and anorthite. S. K. Lee & J. F. Stebbins (2000) reported that most

silicon and aluminum tetrahedra in aluminosilicates are connected by BO to form bonds such as Si–O–Si, Si–O–Al, and Al–O–Al, indicating that the structure only has a few NBOs. Therefore, silica shows higher adsorption energy due to more exposed NBOs. Furthermore, due to the exposure and randomness of NBOs in amorphous substrates, the Na atoms appear to be adsorbed in clusters compared to the more uniform arrangement on crystalline surfaces (Figure 1). This clustering arrangement was present in all silicate cases and was most apparent for silica, where more NBOs can be found on the surface. Together, these results suggest that the silicate composition can affect the adsorption of returning exospheric atoms on planetary surfaces. Simulations and experiments attempting to model planetary cases should, therefore, consider the exact mineral type being studied as opposed to a “representative” silicate.

Our adsorption results on crystalline surfaces also show an increase in adsorption capacity (defined as the percentage of atoms sent toward the surface that then adsorb on the surface) with an increase in temperature, likely due to the increase in kinetic energy of the adsorbate atoms and the increase in adsorption sites present on the surface, as previously shown by M. E. Argun et al. (2007). Furthermore, raising the temperature enhances diffusion, enabling Na atoms to migrate deeper into the substrate and thus allowing space on the surface for additional Na atoms to be accommodated. We note that the exposed surface areas for all cases are approximately the same. Amorphous surfaces, though, exhibit more inconsistent adsorption with a lower adsorption capacity than crystalline surfaces. However, in most cases this increased adsorption energy is caused, in part, by the Na atoms penetrating through the first few angstroms of the randomly rough surface. At the same time, the more exposed uncoordinated O atoms also contribute to the increased energy. We also find that there is very little difference in adsorption energy when altering the temperature compared to changing the composition of the surface. A temperature effect was only present when studying the adsorption of Na on silica at 700 K, which is caused by the atoms penetrating deep within the substrate.

#### 3.2. Diffusion of Sodium throughout the Substrate

In addition to the initial adsorption energy, we also used MD to consider whether, with time, these adsorbates can diffuse to different binding sites, potentially influencing the resulting BE

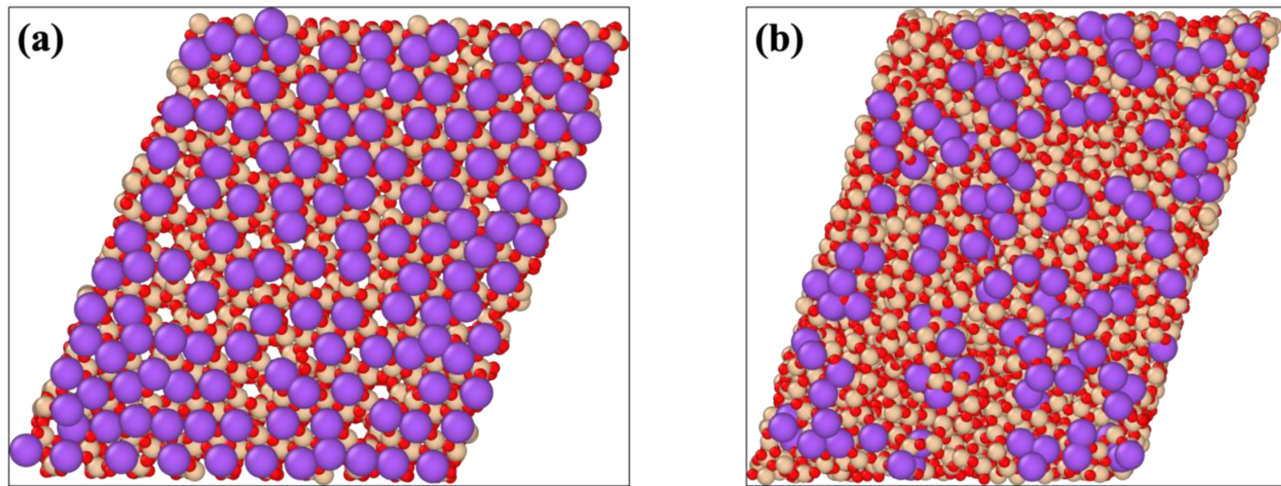


**Figure 1.** Distribution of adsorbed Na atoms on (a) a crystalline and (b) an amorphous silica surface at 100 K. Red particles, O atoms; beige particles, Si atoms; purple particles, Na atoms.

distribution. To establish whether diffusion was occurring, we tracked the Na MSD at the different temperatures simulated (Figure 2). In all cases, we observe an increase in MSD with time, suggesting diffusion of Na. As expected, the MSD of the Na atoms increased with temperature due to the increased kinetic energy of the higher-temperature atoms. At the lowest temperature, we see very little atomic motion, suggesting that the effects of diffusion are limited. In contrast, at 700 K there is a significant increase in the MSD, showing an increased Na mobility at high temperatures. Previous MD simulations have shown that Na diffuses in silicates through a “jumping” mechanism (W. Smith et al. 1995; A. N. Cormack et al. 2002; P. K. Hung et al. 2020). The random nature of this motion suggests that it is important to simulate for long durations to achieve improved statistics, as done here. For crystalline and low-temperature amorphous cases (<300 K), the MSD appears to plateau, suggesting that the more loosely bound adsorbates are diffusing into more tightly bound positions where they can no longer escape.

Figure 2 also further highlights the distinct differences observed between the different mineral types and atomic arrangements. Surprisingly, despite amorphous cases having in general higher mean BE, the MSD for amorphous silicates was always higher than its crystalline counterpart. This suggests that simply tracking the mean BE for a system may be overlooking important processes occurring at the atomic scale. The randomness and different binding sites observed for an amorphous surface likely allows for a proportion of adsorbates to also find lower-BE sites from which they can diffuse further. In contrast, the crystalline minerals are perfectly arranged and thus do not possess these numerous random defects.

Previous experiments on Na ions in amorphous and polycrystalline sodium aluminosilicates showed that the diffusion in the latter is less by a factor of 10 (Z. G. Tyurnina et al. 2015). M. K. Gupta et al. (2020) used ab initio and force-field MD simulations to study the diffusion of Na within  $\text{Na}_2\text{Si}_2\text{O}_5$  bulk. They only observed Na ion diffusion in amorphous structures, while diffusion in crystalline structures was very small, even at temperatures of up to 1100 K. When comparing the amorphous feldspars to amorphous silica, we see that Na mobility is lower for all temperatures simulated in

the presence of Al/Ca and Al/Na contents in anorthite and albite compared to the silica samples. We suspect that this is due to the compositional differences in the silicates, especially during the glass phase (H. Behrens 1992). Competitive interactions for adsorption sites and diffusion pathways are introduced by the presence of elements like Na and Ca in the feldspars. This limits the mobility of adsorbed Na, and thus inhibits the ability to diffuse to higher-BE sites. On the other hand, Na shows improved diffusion and preferential occupation of higher-BE sites in compositionally simpler systems such as  $\text{SiO}_2$ . H. Behrens (1992) studied the diffusion of Na and Ca in plagioclase feldspars, and also found that Na has higher activation energy and lower diffusivity when there is the presence of Ca in the mineral.

For crystalline substrates, adsorbed Na atoms are initially located on surface atoms in all cases (<5 Å). In contrast, for amorphous substrates, a portion of the atoms are located at a depth beyond 5 Å due to the presence of significant surface roughness. With time, we also observe the migration of Na atoms deeper in the substrate for both amorphous and crystalline structures. Such features are significantly more likely at higher temperatures and for amorphous substrates where the Na atoms have more pathways for diffusion. This suggests that diffusion occurs both along the surface and within the substrate. This intra-grain diffusion could introduce a lag in the exospheric release of volatiles on airless bodies (R. M. Killen & T. H. Morgan 1993).

### 3.3. The Effect of Diffusion on the Binding Energy

After establishing diffusion of the adsorbates, we then quantified the mean BE change as a function of simulation time and the number of desorbed Na atoms (Figure 3). First, for the crystalline cases, where MSD was limited, we see only a slight increase in the BE with time. In addition, desorption of Na atoms is only observed in the crystalline silica case at 700 K, where three Na atoms desorb after ~3000 ps. There is, however, a corresponding increase in the mean BE at this moment of desorption, suggesting that the more loosely adsorbed atoms have desorbed. These effects are significantly more pronounced for the amorphous cases, where a comparatively higher MSD of the adsorbed Na was also observed. For

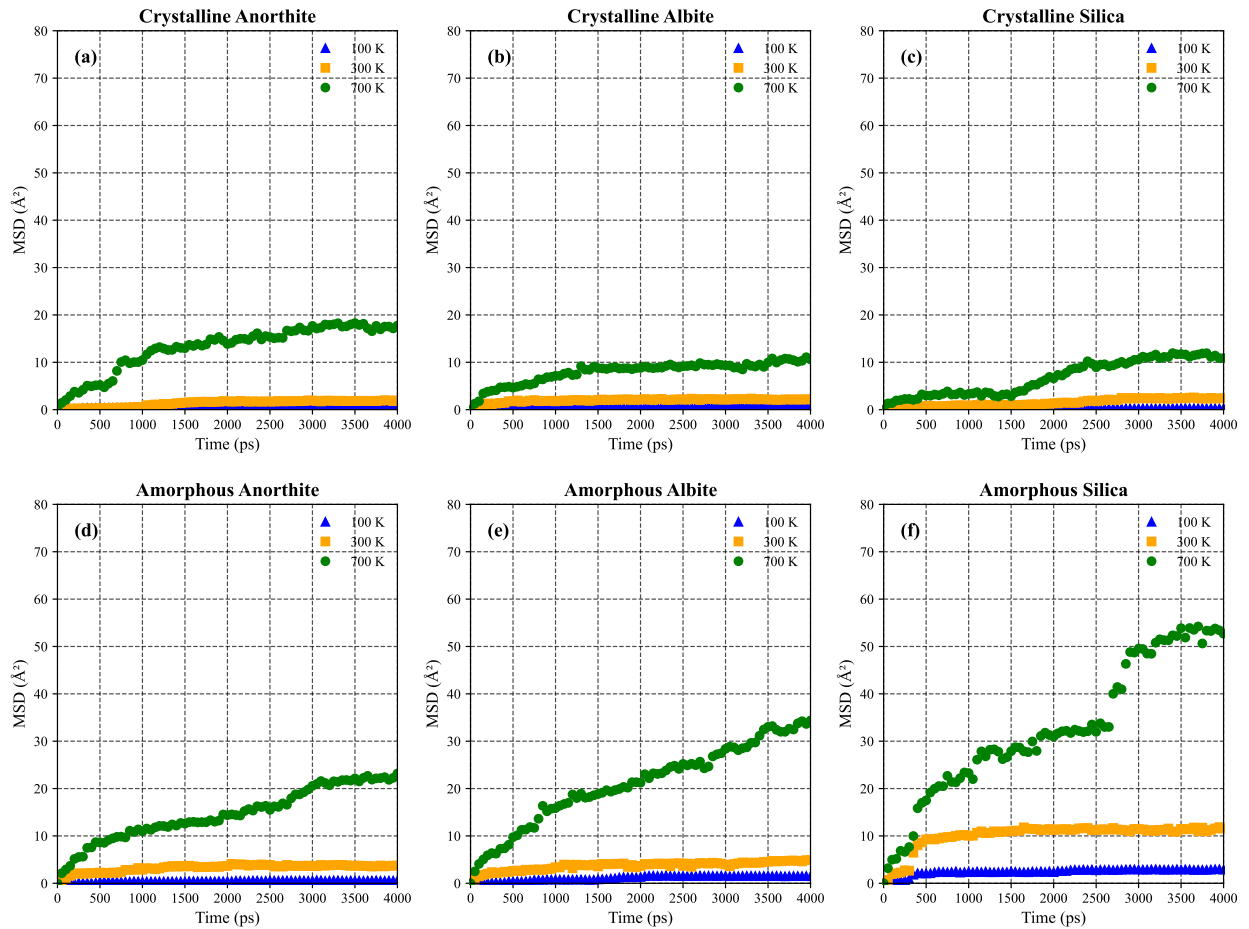


**Figure 2.** Mean squared displacement (MSD) of Na atoms in (a) crystalline anorthite, (b) crystalline albite, (c) crystalline silica, (d) amorphous anorthite, (e) amorphous albite, and (f) amorphous silica.

example, for amorphous albite, we observe a steady increase in the mean BE at 300 K (from 4.3 to 4.6 eV) and 700 K (from 4.4 to 4.8 eV) despite no desorption events occurring. This suggests that adsorbates will diffuse from low- to high-BE sites, eventually increasing the mean BE. This is supported by the very small change in MSD with time as higher-BE sites are encountered and moving away from these tightly bound sites becomes more difficult. As seen in the MSD, there is a significant difference in the behavior of the silica compared to the feldspars. In the beginning, at 300 K and 700 K, there is a slow increase in the mean BE with time as atoms move away from the loosely bound sites. However, with increased time, there are also more desorption events, each resulting in an increase in the mean BE. Therefore, the BE of an adsorbate on a surface is a dynamic value that can be very different from what is sampled at the time of adsorption. With time, the mean BE can increase due to motion toward more tightly bound sites and the desorption of the more loosely bound atoms. Compared to the other silicates, the more rapid diffusion of Na atoms in silica may lead to Na atoms finding their way to very low-BE sites where they can desorb. Based on the temperature of the surface desorption site, the BEs could be as low as 0.0086 eV and 0.06 eV for 100 K and 700 K, respectively.

While the previous results (Figure 3) show the importance of diffusion and time on the BEs, they are limited to mean values. To better understand the underlying mechanisms

causing these changes, Figure 4 shows the normalized distribution of BEs at time zero and after 4000 ps at 100 K. At time zero, we observe a wide range of BEs for the Na atoms for all the cases, with the lowest BE found in crystalline anorthite and amorphous albite at 100 K (1.2 eV) and the highest found in amorphous silica at 700 K (8.8 eV). This suggests that using a singular mean BE to approximate the behavior of adsorbates may overlook important contributions from the high and low end-members. Crystalline substrates show similar BE ranges despite the difference in temperature, with more distinct differences in the BE distribution peaks. For example, when comparing crystalline silica cases, there is a difference of 0.4 eV for the minimum and maximum values between the cases, but the range remains the same. In addition, the peak in the distribution is the same for 100 K and 300 K (4.8 eV) but shows a shift toward higher BE at 700 K (5.2 eV). When comparing the distribution of Na in crystalline and amorphous cases, there is an enhancement of the distribution range for amorphous substrates. This was also observed by L. S. Morrissey et al. (2025), who performed SBE calculations of adsorbed Na on silica surfaces. This is due to the rough surface of the amorphous substrates compared to crystalline, which allows for Na atoms to potentially adsorb deeper in the substrate and bond with more uncoordinated oxygen atoms (L. S. Morrissey et al. 2025).

In all cases, we observe that the BE distribution shifts toward higher values after 4000 ps. By analyzing the BE with

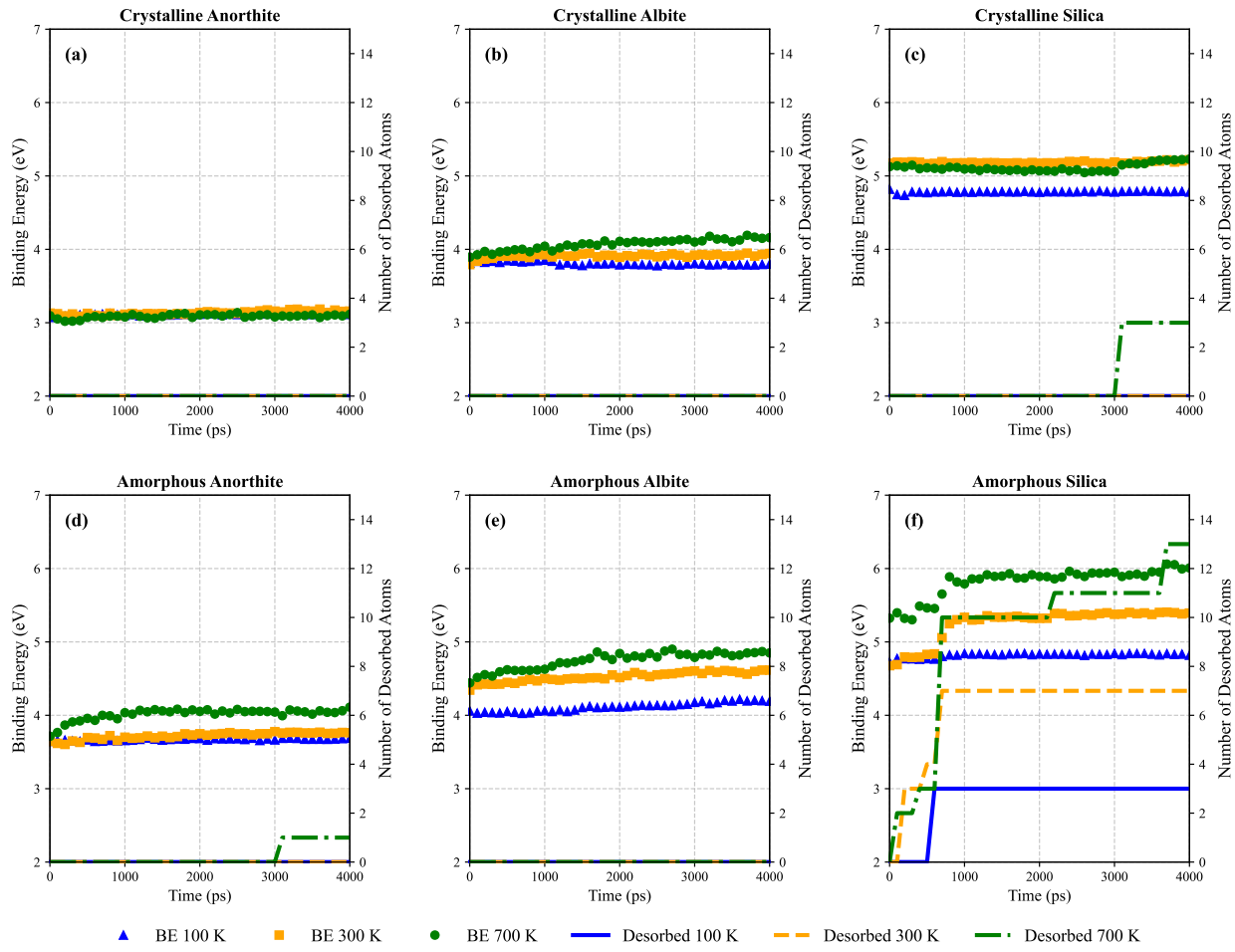


**Figure 3.** Mean binding energy (BE) of Na atoms and number of desorbed Na atoms with time. The shapes represent the BE, whereas the lines represent the desorbed Na atoms.

respect to their location in the substrate, we observe that this shift toward higher-energy binding sites occurs due to Na atoms diffusing both along the surface and deeper within the substrate. Figure 5 shows an example of an initial and final BE of adsorbed atoms on amorphous silica with respect to their location at 700 K and 300 K. Initially, for amorphous silica at 700 K the mean BE at a depth of  $<5 \text{ \AA}$  and  $>5 \text{ \AA}$  is 5.27 eV and 5.67 eV, respectively. At the end of the simulation the BE increased by 16% for atoms located at  $<5 \text{ \AA}$  and by 14% for atoms located at  $>5 \text{ \AA}$ . For amorphous silica at 300 K the average BE showed an increase of 1% for Na atoms located at  $<5 \text{ \AA}$ , with the BE of atoms deeper in the substrate increasing by 25% by the end of the simulation. Therefore, we attribute the increase in Na BE to both surface diffusion and diffusion into the bulk. In addition, for crystalline cases at low temperatures, the Na atoms remain local to the surface (within the first  $\sim 5 \text{ \AA}$ ), suggesting that the BE increase can only be due to surface diffusion to higher-energy binding sites. However, the shift in the overall BE distributions and the fewer number of atoms at low BE ( $<3 \text{ eV}$ ) also suggest that weakly bound atoms desorb and that the atoms that diffuse are now located in more tightly bound adsorption sites. The shift intensifies with increased temperature as the mobility of the atoms increases, allowing them to find higher-BE sites. Morphological changes can also influence the BE distribution; for example, albite starts to transition to the amorphous phase at just below 700 K

(J. Martín-Márquez et al. 2009), meaning that by keeping the temperature for a long time, amorphization will become more intense, enabling diffusion pathways for the adsorbed Na and eventually access to more energetic binding sites.

#### 3.4. Comparison to Previous MD and Experiments

The change in BE distribution with time shows the importance of considering the dynamic nature of key inputs into theoretical global models. L. S. Morrissey et al. (2025) used MD simulations to study the static SBE of Na atoms adsorbed on a silica surface. Unlike our current simulations, the authors simulated a single Na atom with a given kinetic energy, refreshing the surface after each adsorbed atom. This does not consider how the SBE dynamically changes with diffusion. While a direct comparison cannot be made due to the difference between SBE and BE, we find that there is a general overlap in our distributions with that of the authors.

Experimentally, B. V. Yakshinskiy et al. (2000) found that diffusion into the bulk of the  $\text{SiO}_2$  films increases with temperature, which further increases the BE of the Na atoms. The diffusion of Na adsorbates from low-energy to higher-energy sites was also observed experimentally by J. L. McLain et al. (2024). J. L. McLain et al. (2024) also observed Na diffusion at low temperatures of 100 K, which matches our MD simulations well (Figure 5). B. V. Yakshinskiy et al. (2000) also studied the thermal desorption of Na atoms from

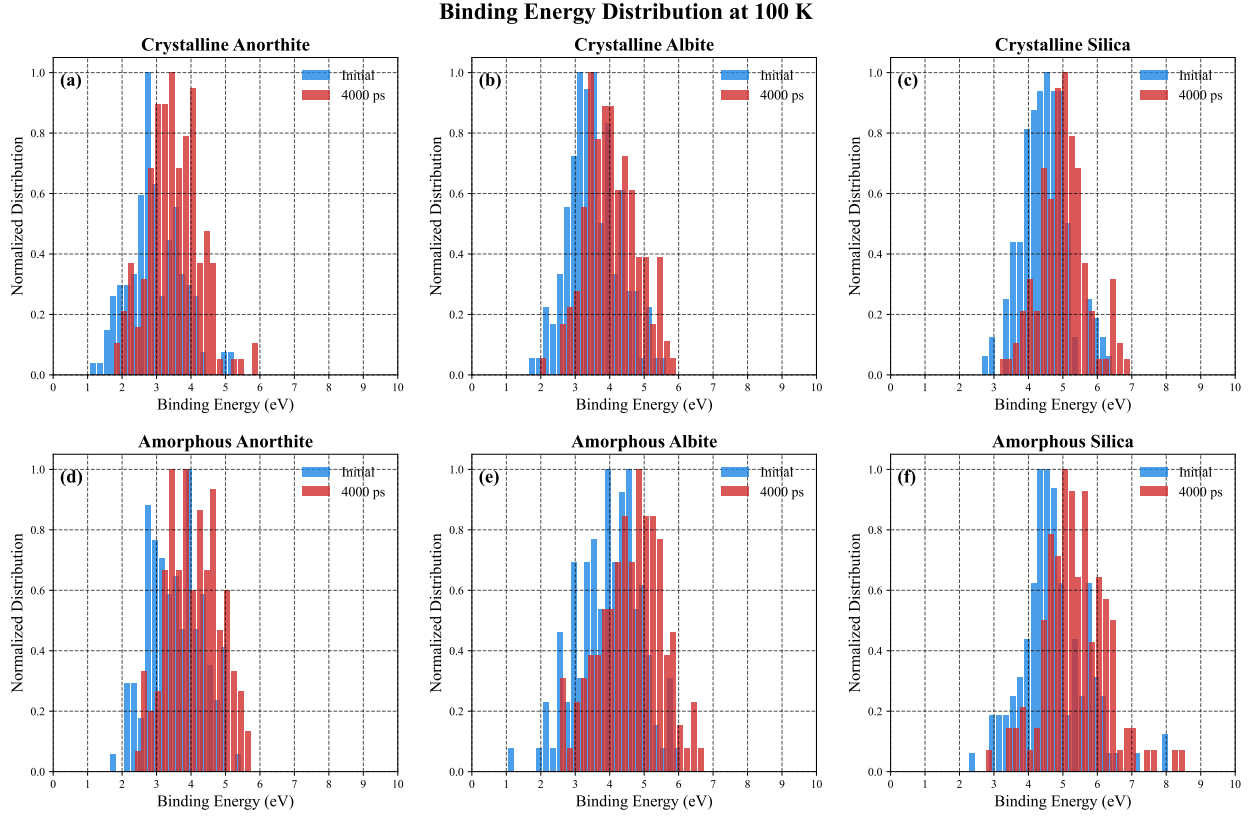


**Figure 4.** Binding energy distribution of Na atoms at 100 K for the different silicates.

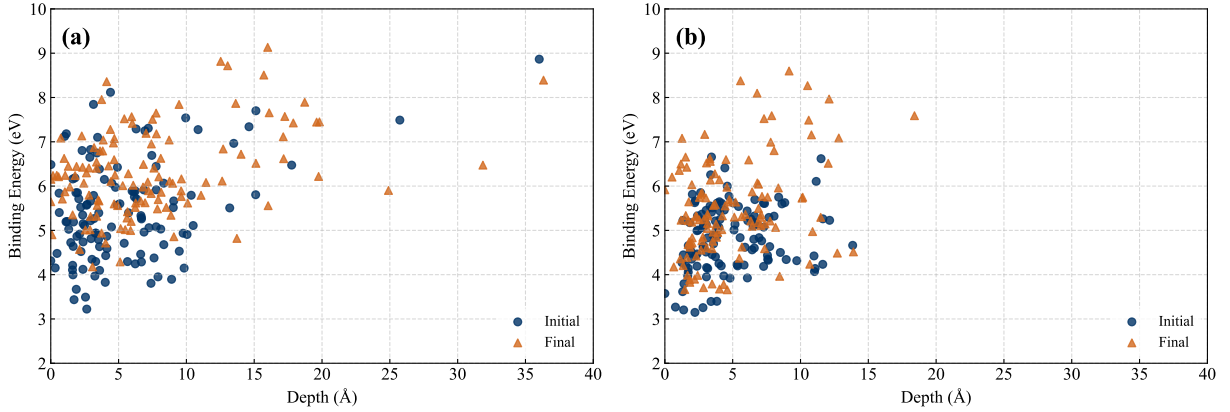


**Figure 5.** Binding energy and depth location of Na atoms on amorphous silica at (a) 700 K and (b) 300 K at the beginning and end of the simulation.

amorphous silica, and found BEs ranging from  $\sim 1.4$  to  $\sim 2.7$  eV atom $^{-1}$ . While our MD simulations showed BEs in that range, we also see much higher BEs of up to  $\sim 9$  eV atom $^{-1}$ . However, experiments are limited by only being able to consider the energy of the desorbed atoms and not that of the adsorbates which remain on the surface. We suggest that the lower BEs measured by B. V. Yakshinskiy et al. (2000) are due to the methodology used to measure the BE of Na. While using temperature-programmed desorption, the authors only accounted for the BE of atoms that desorb and did not consider more strongly bonded atoms on the surface or deeper within the substrate. Here, we show that those atoms which remain on the surface are in more tightly bound sites and that the BEs of desorbed atoms are significantly lower.

#### 4. Implications for Mercury's Surface and Exosphere

The findings of this study can also have several important implications for our understanding of observations of Na and other volatiles on Mercury. Na returning to the surface can be adsorbed at different BEs depending on the surface temperature, composition, and crystal structure. This can create a surface reservoir of adsorbed Na atoms on the nightside of Mercury, where ejected Na is transported through photon pressure from the dayside, as discussed in F. Leblanc & R. E. Johnson (2003, 2010). While T. A. Cassidy et al. (2016) reported that these reservoirs are partially depleted, current exospheric models predict that the Na in the reservoirs is completely ejected due to thermal desorption and PSD. Our results suggest that thermal desorption is more likely to occur in silica-rich

surfaces. However, even then complete depletion of Na could be unlikely due to diffusion of the atoms at high-BE sites and deeper in the surface, where they can be only accessed through solar wind sputtering or micrometeoroid impacts.

T. A. Cassidy et al. (2015) calculated a thermal desorption rate of  $10^{-5} \text{ s}^{-1}$  at Mercury's highest surface temperature. Our results suggest that this depends on the surface composition and crystal structure. For example, at 700 K, amorphous silica experiences the most desorption events, with a desorption rate of  $3.25 \times 10^9 \text{ s}^{-1}$ , while crystalline silica and amorphous anorthite show a desorption rate of  $7.5 \times 10^8 \text{ s}^{-1}$  and  $2.5 \times 10^8 \text{ s}^{-1}$ , respectively. These desorption rates are magnitudes higher than the one calculated by T. A. Cassidy et al. (2015). The discrepancies in our calculated desorption rate and the rate calculated by T. A. Cassidy et al. (2015) are due to the differences in timescale and the BE used to derive the desorption rate. T. A. Cassidy et al. (2015) used a fixed BE of 2.5 eV to derive the desorption rate, which we have shown depends on several factors and dynamically changes with diffusion and time. In addition, while a high BE (up to 9 eV atom $^{-1}$ ) is possible, Na atoms can still randomly diffuse to very low binding sites, leading to their desorption.

Observations have shown that Na emission is higher during the morning than in the afternoon (A. E. A. L. Sprague et al. 1997, 1998; H. Schleicher et al. 2004; A. E. Potter et al. 2006). This was first reported by A. L. Sprague (1992) and has been interpreted as thermal desorption of previously adsorbed Na (T. A. Cassidy et al. 2016). The variation in Na emission throughout the morning and afternoon could be attributed to the change in BE with time. Our results show that an increase in BE can occur at temperatures of 300 K as Na atoms move from more weakly bound sites to stronger binding sites, with desorption events present for adsorbed Na on amorphous silica. As time passes, Na could desorb or fill the higher-BE sites, meaning that even at temperatures of 700 K less Na could be accessible for thermal desorption.

## 5. Conclusions

We have used MD to study the effect of diffusion and temperature on the BE of Na on silicates relevant to the Moon and Mercury. Simulations consider the silicate composition (silica, albite, anorthite), crystal structure (amorphous, crystalline), and diffusion of the adsorbed Na. Results show how the surface composition can influence the initial sampled adsorption energy. The presence of Al/Ca and Al/Na in anorthite and albite, respectively, reduces the adsorption energy of the Na on the silicate, with silica exhibiting the highest energy. In addition, the presence of Al/Ca and Al/Na in the substrate also limits the diffusion of adsorbed Na atoms. We found that diffusion of Na atoms is also reduced in crystalline substrates compared to amorphous ones. The BE has been shown to change with time as diffusion randomly displaces Na atoms to higher-BE sites on the surface and deeper within the substrate. Furthermore, the desorption of loosely bound atoms can also increase the average binding energy. We also sampled the individual BEs of the atoms, showing a wide range of BE distributions that shifted toward higher values after 4000 ps. The results presented emphasize the importance of dynamic processes such as diffusion and their influence on the BE used in global exosphere models. We have shown that the BE can drastically change with time as atoms are allowed to diffuse throughout the substrate. Future studies should expand the current study by considering different surface compositions and adsorbates, such as sulfur and magnesium.

## Acknowledgments

This research was supported by the International Space Science Institute (ISSI) in Bern, through ISSI International Team project #24-616 "Multi-scale Understanding of Surface-Exosphere Connections (MUSEC)." A.G., A.R., and L.M. were supported in part by the NSERC Discovery Grant and the CSA Research Opportunities in Space Sciences program awards.

## ORCID iDs

- Anastasis Georgiou [ID](https://orcid.org/0009-0003-4022-0681) <https://orcid.org/0009-0003-4022-0681>  
 Amanda Ricketts [ID](https://orcid.org/0009-0001-6399-6226) <https://orcid.org/0009-0001-6399-6226>  
 Sébastien Verkerke [ID](https://orcid.org/0000-0002-1966-6553) <https://orcid.org/0000-0002-1966-6553>  
 François Leblanc [ID](https://orcid.org/0000-0002-5548-3519) <https://orcid.org/0000-0002-5548-3519>  
 Menelaos Sarantos [ID](https://orcid.org/0000-0003-0728-2971) <https://orcid.org/0000-0003-0728-2971>  
 Liam S. Morrissey [ID](https://orcid.org/0000-0001-7860-9957) <https://orcid.org/0000-0001-7860-9957>

## References

- Aktulga, H. M., Fogarty, J. C., Pandit, S. A., & Grama, A. Y. 2012, Parallel Reactive Molecular Dynamics: Numerical Methods and Algorithmic Techniques, *ParC*, 38, 245  
 Anthony, J. W., Bideaux, R. A., Bladh, K. W., & Nichols, M. C. 2001, Handbook of Mineralogy (Tucson, AZ: Mineralogical Society of America)  
 Argun, M. E., Dursun, S., Ozdemir, C., & Karatas, M. 2007, Heavy Metal Adsorption by Modified Oak Sawdust: Thermodynamics and Kinetics, *JHzM*, 141, 77  
 Athanasopoulos, D. C., & Garofalini, S. H. 1992, Effect of Adsorption on the Surface Structure of Sodium Alumino-Silicate Glasses: A Molecular Dynamics Simulation, *SurSc*, 273, 129  
 Behrens, H. 1992, Na and Ca Tracer Diffusion in Plagioclase Glasses and Supercooled Melts, *ChGeo*, 96, 267  
 Bida, T. A., & Killen, R. M. 2011, Observations of Al, Fe and Ca + in Mercury's Exosphere, EPSC-DPS Joint Meeting, 6, 1621  
 Bida, T. A., Killen, R. M., & Morgan, T. H. 2000, Discovery of Calcium in Mercury's Atmosphere, *Natur*, 404, 159  
 Broadfoot, A. L., Shemansky, D. E., & Kumar, S. 1976, Mariner 10: Mercury Atmosphere, *GeoRL*, 3, 577  
 Cassidy, T. A., McClintock, W. E., Killen, R. M., et al. 2016, A Cold-pole Enhancement in Mercury's Sodium Exosphere, *GeoRL*, 43, 11  
 Cassidy, T. A., Merkel, A. W., Burger, M. H., et al. 2015, Mercury's Seasonal Sodium Exosphere: MESSENGER Orbital Observations, *Icar*, 248, 547  
 Chakhtouna, H., Benzeid, H., Zari, N., et al. 2023, Microwave-assisted Synthesis of MIL-53(Fe)/Biochar Composite from Date Palm for Ciprofloxacin and Ofloxacin Antibiotics Removal, *Sep. Purif. Technol.*, 308, 122850  
 Chase, S. C., Miner, E. D., Morrison, D., Münch, G., & Neugebauer, G. 1976, Mariner 10 Infrared Radiometer Results: Temperatures and Thermal Properties of the Surface of Mercury, *Icar*, 28, 565  
 Cormack, A. N., Du, J., & Zeitler, T. R. 2002, Alkali Ion Migration Mechanisms in Silicate Glasses Probed by Molecular Dynamics Simulations, *PCCP*, 4, 3193  
 Dal Bó, M., Cantavella, V., Sánchez, E., Hotza, D., & Gilabert, F. A. 2013, Fracture Toughness and Temperature Dependence of Young's Modulus of a Sintered Albite Glass, *JNCS*, 363, 70  
 Domingue, D. L., Chapman, C. R., Killen, R. M., et al. 2014, Mercury's Weather-beaten Surface: Understanding Mercury in the Context of Lunar and Asteroidal Space Weathering Studies, *SSRv*, 181, 121  
 Doressoundiram, A., Leblanc, F., Foellmi, C., & Erard, S. 2009, Metallic Species in Mercury's Exosphere: EMMI/New Technology Telescope Observations, *AJ*, 137, 3859  
 Garofalini, S. H., & Zirl, D. M. 1988, Onset of Alkali Adsorption on the Vitreous Silica Surface, *JVSTA*, 6, 975  
 Gupta, M. K., Mishra, S. K., Mittal, R., et al. 2020, Diffusion of Sodium Ions in Amorphous  $\text{Na}_2\text{Si}_2\text{O}_5$ : Quasielastic Neutron Scattering and Ab Initio Molecular Dynamics Simulations, *PhRvM*, 4, 045802  
 Hajianzadeh, M., Mahmoudi, J., & Sadeghzadeh, S. 2023, Molecular Dynamics Simulations of Methane Adsorption and Displacement from Graphylene Shale Reservoir Nanochannels, *NatSR*, 13, 15765  
 Haynes, W. M. 2014, CRC Handbook of Chemistry and Physics (Boca Raton, FL: CRC Press)

- Hung, P. K., Yen, N. V., Vinh, L. T., et al. 2020, About Hopping Mechanism for Sodium Diffusion in Silicate Liquids with Low Sodium Concentrations: Molecular Dynamics Simulation, *J. Mol. Liq.*, **316**, 113834
- Jäggi, N., Biber, H., Brötzner, J., et al. 2024, SpuBase: Solar Wind Ion Sputter Database for Modeling Purposes, *PSJ*, **5**, 75
- Jain, A., Ong, S. P., Hautier, G., et al. 2013, Commentary: The Materials Project: A Materials Genome Approach to Accelerating Materials Innovation, *APLM*, **1**, 011002
- Killen, R. M., & Morgan, T. H. 1993, Diffusion of Na and K in the Uppermost Regolith of Mercury, *JGR*, **98**, 23589
- Killen, R. M., Morrissey, L. S., Burger, M. H., & Jain, A. 2022, The Influence of Surface Binding Energy on Sputtering in Models of the Sodium Exosphere of Mercury, *PSJ*, **3**, 139
- Killen, R. M., Sarantos, M., Potter, A. E., & Reiff, P. 2004, Source Rates and Ion Recycling Rates for Na and K in Mercury's Atmosphere, *Icar*, **171**, 1
- Leblanc, F., & Johnson, R. E. 2003, Mercury's Sodium Exosphere, *Icar*, **164**, 261
- Leblanc, F., & Johnson, R. E. 2010, Mercury Exosphere I. Global Circulation Model of its Sodium Component, *Icar*, **209**, 280
- Leblanc, F., Sarantos, M., Domingue, D., et al. 2023, How Does the Thermal Environment Affect the Exosphere/Surface Interface at Mercury?, *PSJ*, **4**, 227
- Lee, S. K., & Stebbins, J. F. 2000, Al-O-Al and Si-O-Si Sites in Framework Aluminosilicate Glasses With Si/Al=1: Quantification of Framework Disorder, *JNCS*, **270**, 260
- Liu, P., Liu, J., & Wang, M. 2019, Adsorption of Ethanol Molecules on the Al (1 1 1) Surface: a Molecular Dynamic Study, *RSOS*, **6**, 181189
- Liu, Q., Zhang, X., Jiang, B., et al. 2021, Molecular Dynamics Simulation of Ion Adsorption and Ligand Exchange on an Orthoclase Surface, *ACSoM*, **6**, 14952
- Lyngdoh, G. A., Kumar, R., Krishnan, N. M. A., & Das, S. 2019, Realistic Atomic Structure of Fly Ash-based Geopolymer Gels: Insights from Molecular Dynamics Simulations, *JChPh*, **151**, 64307
- Madey, T. E., Yakshinskiy, B. V., Ageev, V. N., & Johnson, R. E. 1998, Desorption of Alkali Atoms and Ions from Oxide Surfaces: Relevance to Origins of Na and K in Atmospheres of Mercury and the Moon, *JGR*, **103**, 5873
- Martín-Márquez, J., De La Torre, A. G., Aranda, M. A. G., Rincón, J. M., & Romero, M. 2009, Evolution with Temperature of Crystalline and Amorphous Phases in Porcelain Stoneware, *J. Am. Ceram. Soc.*, **92**, 229
- Mayanovic, R. A., Anderson, A. J., Romine, D., & Benmore, C. J. 2023, Insights on the Dissolution of Water in an Albite Melt at High Pressures and Temperatures from a Direct Structural Analysis, *NatSR*, **13**, 4012
- McClintock, W. E., Vervack, R. J., Bradley, E. T., et al. 2009, MESSENGER Observations of Mercury's Exosphere: Detection of Magnesium and Distribution of Constituents, *Sci*, **324**, 610
- McGrath, M. A., Johnson, R. E., & Lanzerotti, L. J. 1986, Sputtering of Sodium on the Planet Mercury, *Natur*, **323**, 694
- McKay, D. S., Heiken, G., Basu, A., et al. 1991, The Lunar Regolith, in *Lunar Sourcebook, A User's Guide to the Moon*, ed. G. H. Heiken et al. (Cambridge: Cambridge Univ. Press), 285
- McLain, J. L., Sarantos, M., Chornay, D., & Dobson, N. 2024, Lunar Sample 62241: Rapid Diffusion and Retention of Adsorbed Sodium and Potassium Atoms, *LPICo*, **3040**, 2489
- Morrison, D. 1970, Thermophysics of the Planet Mercury, *SSRv*, **11**, 271
- Morrissey, L. S., Bringuier, S., Bu, C., et al. 2024, Solar Wind Ion Sputtering from Airless Planetary Bodies: New Insights into the Surface Binding Energies for Elements in Plagioclase Feldspars, *PSJ*, **5**, 272
- Morrissey, L. S., Lewis, J., Ricketts, A., et al. 2025, Theoretical Calculations on the Effect of Adsorbed Atom Coverage on the Sodium Exospheres of Airless Bodies, *ApJ*, **981**, 73
- Morrissey, L. S., Pratt, D., Farrell, W. M., et al. 2022a, Simulating the Diffusion of Hydrogen in Amorphous Silicates: A "Jumping" Migration Process and its Implications for Solar Wind Implanted Lunar Volatiles, *Icar*, **379**, 114979
- Morrissey, L. S., Tucker, O. J., Killen, R. M., Nakhla, S., & Savin, D. W. 2022, Solar Wind Ion Sputtering of Sodium from Silicates Using Molecular Dynamics Calculations of Surface Binding Energies, *ApJL*, **925**, L6
- Nhan, N. T., Lien, P. T., Kien, P. H., San, L. T., & Hung, P. K. 2024, Study of Diffusion in Sodium Silicate Glass Using Molecular Dynamics Simulation, *Silicon*, **16**, 5571
- Pallini, A., Bertani, M., Rustichelli, D., et al. 2023, Comparison of Five Empirical Potential Models for Aluminosilicate Systems: Albite and Anorthite As Test Cases, *JNCS*, **615**, 122426
- Pitman, M. C., & Van Duin, A. C. T. 2012, Dynamics of Confined Reactive Water in Smectite Clay-Zeolite Composites, *JChS*, **134**, 3042
- Plimpton, S. 1995, Fast Parallel Algorithms for Short-Range Molecular Dynamics, *JCoPh*, **117**, 1
- Potter, A., & Morgan, T. 1985, Discovery of Sodium in the Atmosphere of Mercury, *Sci*, **229**, 651
- Potter, A. E., Killen, R. M., & Sarantos, M. 2006, Spatial Distribution of Sodium on Mercury, *Icar*, **181**, 1
- Potter, A. E., & Morgan, T. H. 1986, Potassium in the Atmosphere of Mercury, *Icar*, **67**, 336
- Quadery, A. H., Pacheco, S., Au, A., et al. 2015, Atomic-scale Simulation of Space Weathering in Olivine and Orthopyroxene, *JGRE*, **120**, 643
- Quémerais, E., Koutroumpa, D., Lallement, R., et al. 2023, Observation of Helium in Mercury's Exosphere by PHEBUS on Bepi-Colombo, *JGRE*, **128**, e2023JE007743
- Rarivomanantsoa, M., Jund, P., & Jullien, R. 2004, Sodium Diffusion through Amorphous Silica Surfaces: A Molecular Dynamics Study, *JChPh*, **120**, 4915
- Robidel, R., Quémerais, E., Chaufray, J. Y., et al. 2023, Mercury's Exosphere as Seen by BepiColombo/PHEBUS Visible Channels during the First Two Flybys, *JGRE*, **128**, e2023JE007808
- Sarantos, M., & Tsavachidis, S. 2020, The Boundary of Alkali Surface Boundary Exospheres of Mercury and the Moon, *GeoRL*, **47**, e2020GL088930
- Schleicher, H., Wiedemann, G., Wöhrl, H., Berkefeld, T., & Soltau, D. 2004, Detection of Neutral Sodium Above Mercury during the Transit on 2003 May 7, *A&A*, **425**, 1119
- Senftle, T. P., Hong, S., Islam, M. M., et al. 2016, The ReaxFF Reactive Force-field: Development, Applications and Future Directions, *npjCM*, **2**, 15011
- Sheikholeslam, S. A., Manzano, H., Grecu, C., & Ivanov, A. 2016, Reduced Hydrogen Diffusion in Strained Amorphous SiO<sub>2</sub>: Understanding Ageing in MOSFET Devices, *JMCC*, **4**, 8104
- Smith, W., Greaves, G. N., & Gillan, M. J. 1995, Computer Simulation of Sodium Disilicate Glass, *JChPh*, **103**, 3091
- Sprague, A. L. 1992, Mercury's Atmospheric Bright Spots and Potassium Variations: A Possible Cause, *JGR*, **97**, 18257
- Sprague, A. L., Kozlowski, R. W. H., Hunten, D. M., et al. 1997, Distribution and Abundance of Sodium in Mercury's Atmosphere, 1985–1988, *Icar*, **129**, 506
- Sprague, A. L., Kozlowski, R. W. H., Witteborn, F. C., Cruikshank, D. P., & Wooden, D. H. 1994, Mercury: Evidence for Anorthosite and Basalt from Mid-infrared (7.3–13.5 μm) Spectroscopy, *Icar*, **109**, 156
- Sprague, A. L., Schmitt, W. J., & Hill, R. E. 1998, Mercury: Sodium Atmospheric Enhancements, Radar-bright Spots, and Visible Surface Features, *Icar*, **136**, 60
- Taylor, M., & Brown, G. E. 1979, Structure of Mineral Glasses—I. The Feldspar Glasses NaAlSi<sub>3</sub>O<sub>8</sub>, KAlSi<sub>3</sub>O<sub>8</sub>, CaAl<sub>2</sub>Si<sub>2</sub>O<sub>8</sub>, *GeCoA*, **43**, 61
- Thakur, A., Assad, H., Kaya, S., & Kumar, A. 2022, Plant Extracts as Environmentally Sustainable Corrosion Inhibitors II, Eco-friendly Corrosion Inhibitors: Principles, Designing and Applications (New York: Elsevier), 283
- Thao, N. T., Yen, N. V., & Lien, P. T. 2023, Diffusion Behaviors of Sodium Atoms within Si-O Network in Sodium Silicate Glasses: Insights from Molecular Dynamics Simulations, *EPJB*, **96**, 138
- Tyurnina, Z. G., Tyurnina, N. G., & Sviridov, S. I. 2015, Diffusion of Sodium Ions and Electric Conductivity in Glassy and Crystallized Na<sub>2</sub>O · Al<sub>2</sub>O<sub>3</sub> · 2SiO<sub>2</sub>, *Glass Phys. Chem.*, **41**, 579
- Van Duin, A. C. T., Dasgupta, S., Lorant, F., & Goddard, W. A. 2001, ReaxFF: A Reactive Force Field for Hydrocarbons, *JPCA*, **105**, 9396
- Vasavada, A. R., Paige, D. A., & Wood, S. E. 1999, Near-surface Temperatures on Mercury and the Moon and the Stability of Polar Ice Deposits, *Icar*, **141**, 179
- Verkerke, S., Leblanc, F., Chaufray, J.-Y., et al. 2024, Sodium Enrichment of Mercury's Subsurface Through Diffusion, *GeoRL*, **51**, e2024GL109393
- Vervack, R. J., Killen, R. M., McClintock, W. E., et al. 2016, New Discoveries from MESSENGER and Insights into Mercury's Exosphere, *GeoRL*, **43**, 11
- Vervack, R. J., McClintock, W. E., Killen, R. M., et al. 2010, Mercury's Complex Exosphere: Results from MESSENGER's Third Flyby, *Sci*, **329**, 672
- Wurz, P., Whitby, J. A., Rohner, U., et al. 2010, Self-consistent Modeling of Mercury's Exosphere by Sputtering, Micro-meteorite Impact and Photon-stimulated Desorption, *P&SS*, **58**, 1599
- Yakshinskiy, B. V., & Madey, T. E. 2003, DIET of Alkali Atoms from Mineral Surfaces, *SurSc*, **528**, 54
- Yakshinskiy, B. V., Madey, T. E., & ageev, V. N. 2000, Thermal Desorption of Sodium Atoms from Thin SiO<sub>2</sub> Films, *SRL*, **7**, 75
- Yu, Y., Wang, B., Wang, M., Sant, G., & Bauchy, M. 2017, Reactive Molecular Dynamics Simulations of Sodium Silicate Glasses—Toward an Improved Understanding of the Structure, *IIG*, **8**, 276
- Zirl, D. M., & Garofalini, S. H. 1990, Structure of Sodium Aluminosilicate Glasses, *J. Am. Ceram. Soc.*, **73**, 2848